Evaluation of DIII-D plasmas for Future Measurements of the Driven Current Density in the DIII-D High Field Side Lower Hybrid Experiment

Grant Rutherford[1,*], *Mirela* Cengher[1], *Ivan* Garcia[1], *Malcolm* Gould[1], *Evan* Leppink[1], *Yijun* Lin[1], *Samuel* Pierson[1], *James* Ridzon[1], *Andrew H.* Seltzman[1], *Brian S.* Victor[2], and *Stephen J.* Wukitch[1]

[1]Massachusetts Institute of Technology, Plasma Science and Fusion Center
[2]Lawrence Livermore National Laboratory

Abstract. High field side (HFS) lower hybrid current drive (LHCD) is a promising method for efficiently driving off-axis current in steady state tokamak power plants. The first test of this technology is underway at the DIII-D tokamak. The initial physics goal is to measure the LH-driven current density profile in order to validate the ray-tracing/Fokker-Plank codes GENRAY/CQL3D and gain confidence in their ability to predict LH deposition in future DIII-D experiments and fusion power plants. DIII-D's motional Stark effect (MSE) diagnostic will be used to constrain the magnetic equilibrium reconstructions. From these reconstructions, the ohmic, bootstrap, and driven non-inductive components of the current density profile can be extracted. Several recent DIII-D plasmas have been identified in which GENRAY/CQL3D predict measurable amounts of current with only 100 kW of coupled power.

1 Introduction

Efficient, non-inductive current drive is a requirement for steady state tokamak power plants and can be beneficial to pulsed schemes as well. Lower hybrid current drive (LHCD) has been demonstrated as a highly efficient current drive scheme [1]. However all prior LH experiments have launched the waves from the low field side (LFS) of the tokamak. This places the launcher in the path of the majority of the heat flux leaving the plasma, reducing the launcher's survivability.

By moving the lower hybrid launcher to the high field side (HFS), not only is the heat flux much lower, but there are several physics benefits as well. The higher local magnetic field permits the use of a smaller parallel refractive index $N_\|$ due to the requirement that $|N_\|| > N_{acc}$ in order to prevent mode conversion to the fast branch of the dispersion relation, where N_{acc} scales with 1/B:

$$|N_\|| > N_{\text{acc}} \approx \frac{\omega_{pe}}{\Omega_e} + \sqrt{1 - \frac{\omega_{pi}^2}{\omega^2} + \frac{\omega_{pe}^2}{\Omega_e^2}} \propto \frac{\sqrt{n_e}}{B}, \qquad (1)$$

where ω_{pe} is the electron plasma frequency, ω_{pi} is the ion plasma frequency, Ω_e is the electron cyclotron frequency, ω is the wave angular frequency, n_e is the electron density, and B is the total magnetic field. Additionally, the HFS scrape-off layer (SOL) is more quiescent than the LFS SOL, which is expected to simplify coupling and reduce parasitic interactions between the SOL and the LH waves, which have been shown to decrease current drive efficiency [2–4].

The first test of HFS LHCD [5] is underway on the DIII-D tokamak. The HFS LHCD launcher was optimized to launch an $|N_\|| = 2.7$ (sign dependent on the direction of the magnetic field) at 4.6 GHz and is expected to couple up to a total of ~1.5 MW to the plasma across all lobes [6]. The launcher consists of eight modules in the toroidal direction (each with six apertures toroidally and four apertures poloidally). By varying the klystron phasing, the launcher can produce spectra that peak at $|N_\||$ between 2.3 and 3.1. At the time of writing, the launcher is being conditioned. Once sufficient power and pulse length is reached, the initial physics task is to measure the driven current density profile. This is critical for validating that the ray-tracing/Fokker-Planck codes GENRAY [7]/CQL3D [8] are sufficiently accurate to be used in the design of future DIII-D experiments and fusion power plants.

Measurement of the HFS LH driven current density profile will be conducted using DIII-D's motional Stark effect (MSE) system, which consists of 5 arrays totaling 65 channels [9]. MSE measures the pitch of the local magnetic field via Stark splitting of atomic energy levels due to the electric field $E = \vec{v} \times \vec{B}$ that appears in the frame of an atom as it moves in the tokamak. Via the polarization of the emitted radiation, the pitch of $\vec{B}$ can be resolved [10]. This measurement requires neutral particles with high velocities at the location of interest, which are provided by neutral beam injection. The magnetic field pitch information is then fed into the magnetic equilibrium code EFIT [11] to constrain the reconstructions.

The remainder of the analysis consists of identifying and subtracting off portions of the current profile from

*Corresponding author: rantr@mit.edu

the total parallel current density $J_{\parallel}$, producing the non-inductive current density of interest. The bulk electron ohmic contribution is given by $J_{\mathrm{ohm}}(\rho) = \sigma_{neo}(\rho)E_{\parallel}(\rho)$, where $\rho = \sqrt{\phi/(\pi B_{T0})}$ is an effective radius with units meters, ϕ is the toroidal flux, B_{T0} is the magnetic field on-axis, σ_{neo} is the neoclassical conductivity, and $E_{\parallel}$ is the parallel electric field generated inductively via the central solenoid. σ_{neo} is calculated with the Python package omfit-classes' nclass_conductivity method [12] with the average ion charge number 'Koh' option, as derived in [13].

$E_{\parallel}$ is calculated via [14]:

$$E_{\parallel} = -\frac{\langle B_{\phi}^2 \rangle}{F B_{T0}} \frac{d\psi}{dt}\bigg|_{\phi}, \tag{2}$$

where $\langle B_{\phi}^2 \rangle$ is a flux surface average of the square of the toroidal magnetic field, F is the normalized poloidal current $\int_0^R R J_z dR$, and ψ is the poloidal flux. When ρ_b, the value of ρ at the separatrix, or B_{T0} are functions of time, the following can be used:

$$\frac{d\psi}{dt}\bigg|_{\phi} = \frac{d\psi}{dt}\bigg|_{\hat{\rho}} - \frac{B_{T0}\rho_b^2\hat{\rho}^2}{q}\left(\frac{1}{\rho_b}\frac{d\rho_b}{dt} + \frac{1}{2B_{T0}}\frac{dB_{T0}}{dt}\right), \tag{3}$$

where $\hat{\rho} = \rho/\rho_b$.

The bootstrap contribution J_{BS} is calculated with omfit-classes's sauter_bootstrap method, again taking the 'Koh' [13] option for the average ion charge number. The driven non-inductive current is then given by $J_{\mathrm{NI}} = J_{\parallel} - J_{\mathrm{ohm}} - J_{\mathrm{BS}} = J_{\mathrm{NB}} + J_{\mathrm{EC}} + J_{\mathrm{LH,tot}}$, where J_{NB} is the neutral beam current density, and J_{EC} is the electron cyclotron current density. This process is then repeated for a reference shot with zero LH power applied. Assuming the plasma profiles and other current drive sources are approximately unchanged, $J_{\mathrm{LH,tot}}$ can be found via $J_{\mathrm{NI}} - J_{\mathrm{NI,\,ref}}$.

$J_{\mathrm{LH,tot}} = J_{\mathrm{LH}} + J_{\mathrm{hot}}$, where J_{LH} is current density due to the LH waves driving fast electrons, and J_{hot} is the current density due to the synergistic effect between $E_{\parallel}$ and the LH-driven fast electrons [15]. To determine the magnitude of these two terms from the measured $J_{\mathrm{LH,tot}}$, a model for the hot conductivity σ_1, such as that given in [16], could be used to find $J_{\mathrm{hot}} = \sigma_1 E_{\parallel}$. Alternatively, GENRAY/CQL3D simulations could be completed with just $E_{\parallel}$, with just LH, and with both LH and $E_{\parallel}$. By comparing the driven currents in these three cases, the expected J_{LH} and J_{hot} could be identified. The simulations detailed in the following Section do not include any electric field and are thus conservative estimates of the driven current.

If it is found that the plasma profiles do change between the reference plasma and the plasma with LH, it will likely be due to the difference in auxiliary power. One of the electron cyclotron systems could be used in heating mode to account for this. This analysis requires a quiescent flattop of ideally several hundred ms and favors high B (~2T on DIII-D) to maximize Stark splitting and thus the MSE signal. An upper bound on the smallest measurable current density comes from [17], where a current density profile with a $J_{\mathrm{CD,peak}}$ of 70 kA/m^2 was successfully measured.

Table 1. Shot number, time slice, toroidal magnetic field, and plasma current for three possible MSE current drive measurement target plasmas.

Shot	time (ms)	B_0 (T)	I_p (MA)
203692	2300	1.97	1.37
199749	3000	-1.99	1.37
195187	1300	1.87	1.0

2 Predictions of HFS LH current density

GENRAY/CQL3D simulations have been performed for several DIII-D plasmas to identify target shots in which the desired peak J_{LH} is achievable. Given that this measurement will be attempted during the first campaign in which the LH launcher is operational, not all modules may be sufficiently conditioned for use. As such, the GENRAY/CQL3D simulations were completed assuming low power and only three neighboring modules. All GENRAY simulations assumed four poloidal launch points, matching the four-way poloidal splitting of the launcher. The three most powerful lobes were included using a $\sin(x)^2/x^2$ power spectrum, where $x = 2\pi(N_{\parallel,peak} - 0.5\Delta N_{\parallel})/\Delta N_{\parallel}$ and $\Delta N_{\parallel}$ is the zero-crossing width of the lobe. Additionally, a modified version of GENRAY's hot plasma dispersion relation was used that includes the hot plasma correction to $\epsilon_{\parallel}$ [18].

The GENRAY/CQL3D results for three target shots are presented here. The timeslices, toroidal magnetic field, and plasma current of these shots are listed in Table 1. These shots were chosen due to their low density and high temperature, which maximize the current driven at small power levels. All simulations were completed assuming 100 kW of power is coupled to the plasma. The effect of the $E_{\parallel}$ on the driven current is neglected.

203692 is an L-mode plasma used in a previous HFS LHCD conditioning experiment, where it showed low reflected power in the LH transmission lines. The temperature and density profiles are given in Figure 1, the predicted LH-driven current density profiles are shown in Figure 2, and Figure 3 is an example of the ray-trajectories for the $N_{\parallel} = -2.7$ case. All of the cases except $N_{\parallel} = -2.5$ surpass the needed 70 kA/m^2. Additionally, this range of $N_{\parallel}$ exhibits single pass damping, decreasing the likelihood of SOL interactions decreasing simulation accuracy, which may occur due to GENRAY/CQL3D not having knowledge of the SOL.

However, there is some sawtoothing in 203692 during flattop, which would negatively affect the MSE analysis. It is therefore planned to decrease the plasma current from 1.37 MA to 1 MA when conducting the MSE experiment. How this reduction in plasma current affects the waves' upshift was approximated by repeating the GENRAY/CQL3D simulations with the same profiles and toroidal field but scaling poloidal field down by a factor of 1/1.37. The new current density profiles are shown in Figure 4, where both $N_{\parallel} = -2.5$ and -2.7 fall below the target value of $J_{\mathrm{LH,peak}} \geq 70$ kA/m^2. Interestingly, the shapes of the $N_{\parallel} = -2.9$ and -3.1 current density profiles are simpler than in the $I_p = 1.37$ MA case and would be more easily

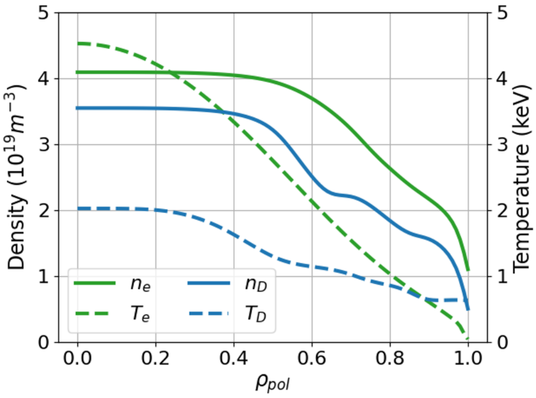

Figure 1. Temperature and density for DIII-D discharge 203692.

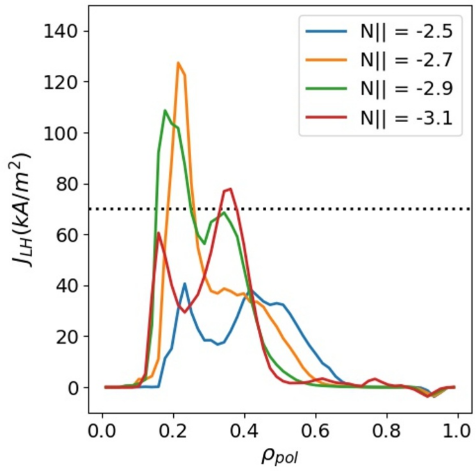

Figure 2. LH current density profile predictions for shot 203692 for various launched $N_\parallel$ and 100 kW of coupled LH power.

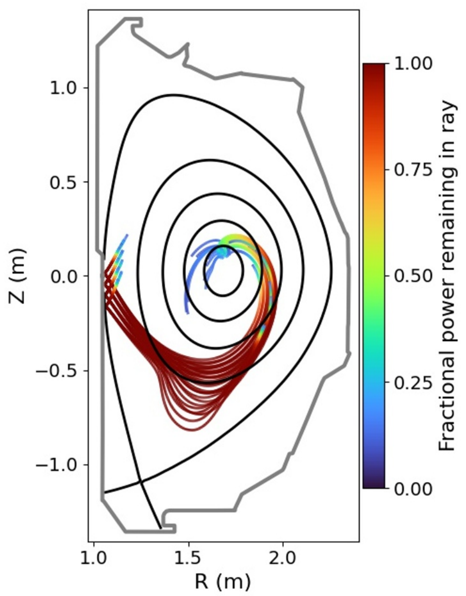

Figure 3. Ray-trajectories predicted for shot 203692 for $N_\parallel = -2.7$.

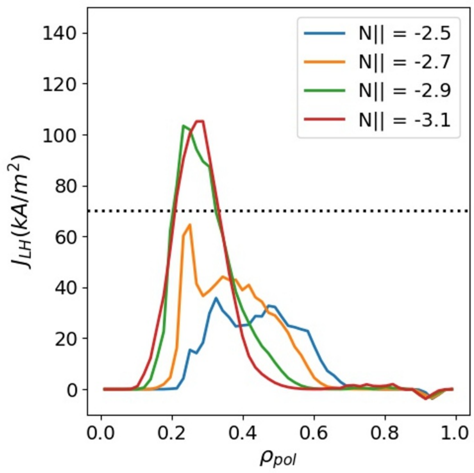

Figure 4. LH current density profile predictions for an $I_p = 1$ MA version of 203692 for various launched $N_\parallel$ and 100 kW of coupled LH power.

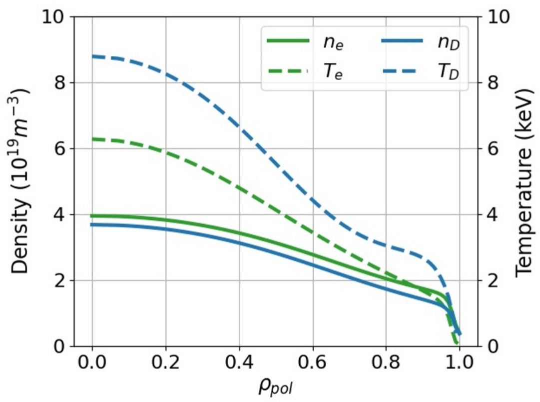

Figure 5. Temperature and density profiles for DIII-D discharge 199749.

reproduced by the MSE analysis. In the case that reducing the plasma current does not sufficiently prevent the onset of sawteeth during the desired measurement window, averaging over many sawtooth periods or over multiple repeat shots may be attempted to improve the measurement.

199749 is an H-mode plasma from an ELM suppression experiment that made use of resonant magnetic perturbations (RMPs), resulting in low density (see Figure 5). Looking to Figure 6, more current is expected to be driven in 199749 than 203692. Like 203692, this range of $N_\parallel$ is in the single pass absorption regime. While the larger driven current densities are beneficial, 199749 is far more sensitive to wall conditions than 203692. In a previous launcher conditioning experiment, it was attempted to reproduce 199749, but the low density could not be achieved. 199749 also features sawteeth similar to 203692.

195187 is an L-mode plasma from a helicon experiment. From 1100 ms - 1500 ms, 195187 is quite quiescent and presents a good time period for the MSE measurement. The temperature and density profiles are shown in Figure 7, and the predicted current densities are given in Figure 8. All cases readily surpass the desired 70 kA/m^2 value, though the single pass absorptions are 97%, 71%, 41%, and 56% for $N_\parallel = -2.5$, -2.7, -2.9, and -3.1,

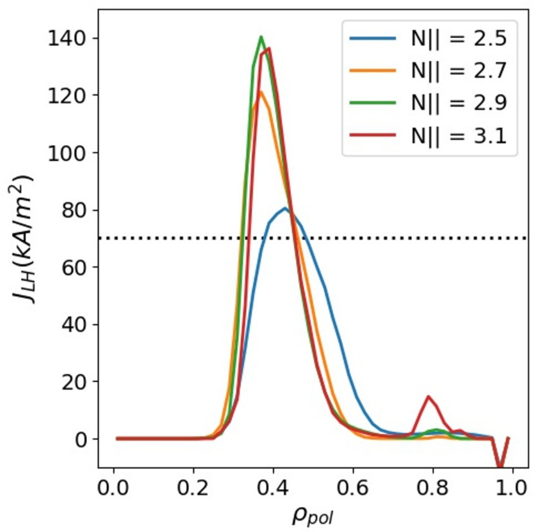

Figure 6. LH current density profile predictions for shot 199749 for various launched $N_{\parallel}$ and 100 kW of coupled LH power.

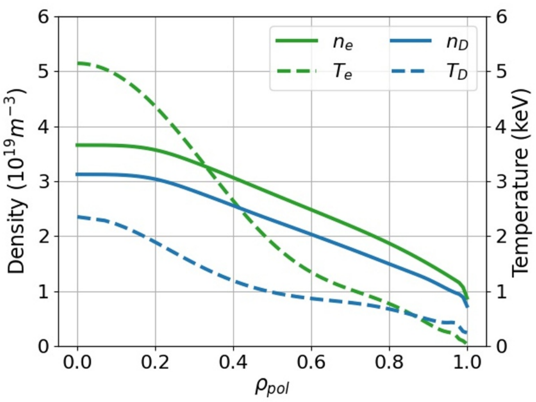

Figure 7. Temperature and density profiles for DIII-D discharge 195187.

respectively. While closer to the multipass regime than 203692 or 199749, these values are still well in excess of the typical single pass absorption in past LHCD experiments on other devices.

3 Conclusion

Conditioning of the HFS LHCD launcher is underway at DIII-D. When it is possible to couple 100 kW to the plasma, several DIII-D discharges have been identified in which the predicted LH current density is larger than the current density successfully measured in past electron cyclotron top launch experiments.

Acknowledgements

The authors would like to thank Craig Petty and Jeff Lestz for many useful discussions about the details of MSE current density measurements. This material is based upon work supported by the U.S. Department of Energy, Office of Science, Office of Fusion Energy Sciences, using the DIII-D National Fusion Facility, a DOE Office of Science user facility, under Awards DE-SC0014264 and DE-FC02-04ER54698. This work is also supported by US DoE Contract No. DE-FC02-01ER54648 under a Scientific Discovery through Advanced Computing Initiative. Disclaimer: This report was prepared as an account of work sponsored by an agency of the United States Government. Neither the United States Government nor any agency thereof, nor any of their employees, makes any warranty, express or implied, or assumes any legal liability or responsibility for the accuracy, completeness, or usefulness of any information, apparatus, product, or process disclosed, or represents that its use would not infringe privately owned rights. Reference herein to any specific commercial product, process, or service by trade name, trademark, manufacturer, or otherwise does not necessarily constitute or imply its endorsement, recommendation, or favoring by the United States Government or any agency thereof. The views and opinions of authors expressed herein do not necessarily state or reflect those of the United States Government or any agency thereof.

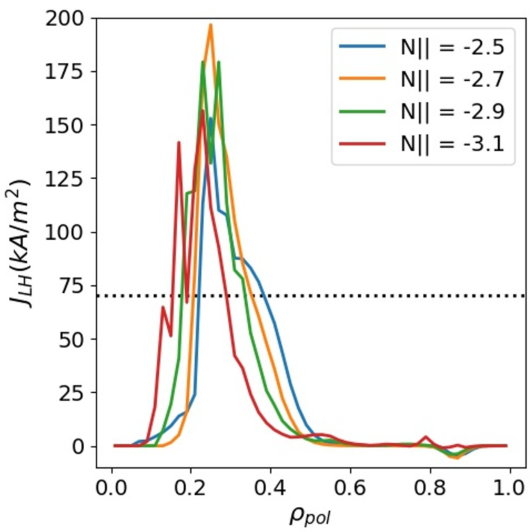

Figure 8. LH current density profile predictions for shot 195187 for various launched $N_{\parallel}$ and 100 kW of coupled LH power.

References

[1] A. Bécoulet et al., Steady state long pulse tokamak operation using lower hybrid current drive, Fusion Engineering and Design **86**, 490 (2011), proceedings of the 26th Symposium of Fusion Technology (SOFT-26). https://doi.org/10.1016/j.fusengdes.2011.01.098

[2] G. Wallace, A. Hubbard, P. Bonoli et al., Lower hybrid current drive at high density in Alcator C-Mod, Nuclear Fusion **51**, 083032 (2011). https://dx.doi.org/10.1088/0029-5515/51/8/083032

[3] B. Ding, P. Bonoli, A. Tuccillo et al., Review of recent experimental and modeling advances in the understanding of lower hybrid current drive in ITER-relevant regimes, Nuclear Fusion **58**, 095003 (2018). https://doi.org/10.1088/1741-4326/aad0aa

[4] I.C. Faust, D. Brunner, B. LaBombard et al., Lower hybrid wave edge power loss quantification on the Alcator C-Mod tokamak, Physics of Plasmas **23**, 056115 (2016). https://doi.org/10.1063/1.4951736

[5] A. Seltzman, S. Shiraiwa, G. Wallace, S. Wukitch, A high field side multijunction launcher with aperture impedance matching for lower hybrid current drive in DIII-D advanced tokamak plasmas, Nuclear Fusion **59**, 096003 (2019). https://doi.org/10.1088/1741-4326/ab22c8

[6] A. Seltzman, S. Wukitch, RF losses in selective laser melted GRCop-84 copper waveguide for an additively manufactured lower hybrid current drive launcher, Fusion Engineering and Design **159**, 111762 (2020). https://doi.org/10.1016/j.fusengdes.2020.111762

[7] A. Smirnov, R. Harvey, Calculations of the current drive in DIII-D with the genray ray tracing code, Bull. Am. Phys. Soc **40**, 35 (1995).

[8] R. Harvey, M. McCoy, The cql3d fokker-planck code, Proceedings of the IAEA Technical Committee Meeting on Simulation and Modeling of Thermonuclear Plasmas pp. 489–526 (1992).

[9] C.T. Holcomb, S.L. Allen, M.A. Makowski et al., An overview of the motional Stark effect diagnostic on DIII-D and design work for an ITER MSE, AIP Conference Proceedings **988**, 214 (2008). https://doi.org/10.1063/1.2905070

[10] F.M. Levinton, The motional Stark effect: Overview and future development (invited), Review of Scientific Instruments **70**, 810 (1999). https://doi.org/10.1063/1.1149316

[11] L. Lao, J. Ferron, R. Groebner et al., Equilibrium analysis of current profiles in tokamaks, Nuclear Fusion **30**, 1035 (1990). https://doi.org/10.1088/0029-5515/30/6/006

[12] O. Meneghini, S. Smith, L. Lao et al., Integrated modeling applications for tokamak experiments with OMFIT, Nuclear Fusion **55**, 083008 (2015). https://doi.org/10.1088/0029-5515/55/8/083008

[13] S. Koh, C.S. Chang, S. Ku, J.E. Menard, H. Weitzner, W. Choe, Bootstrap current for the edge pedestal plasma in a diverted tokamak geometry, Physics of Plasmas **19**, 072505 (2012). https://doi.org/10.1063/1.4736953

[14] C.B. Forest, K. Kupfer, T.C. Luce et al., Determination of the noninductive current profile in tokamak plasmas, Phys. Rev. Lett. **73**, 2444 (1994). https://doi.org/10.1103/PhysRevLett.73.2444

[15] G. Giruzzi, E. Barbato, S. Bernabei, A. Cardinali, Measurement of the hot electrical conductivity in the PBX-M tokamak, Nuclear Fusion **37**, 673 (1997). https://doi.org/10.1088/0029-5515/37/5/I09

[16] N.J. Fisch, Conductivity of rf-heated plasma, The Physics of Fluids **28**, 245 (1985). https://doi.org/10.1063/1.865186

[17] X. Chen, C. Petty, J. Lohr et al., Doubling off-axis electron cyclotron current drive efficiency via velocity space engineering, Nuclear Fusion **62**, 054001 (2022). https://doi.org/10.1088/1741-4326/ac544a

[18] S.J. Frank, J.C. Wright, I.H. Hutchinson, P.T. Bonoli, An assessment of full-wave effects on maxwellian lower-hybrid wave damping, Plasma Physics and Controlled Fusion **64**, 105023 (2022). https://doi.org/10.1088/1361-6587/ac89ae